Origin of the Patchy Emission Pattern at the ZERT CO_2 Release Test

Curtis M. Oldenburg[1]

Jennifer L. Lewicki[1]

Lehua Pan[1]

Laura Dobeck[2]

Lee Spangler[2]

[1]Earth Sciences Division 90-1116

Lawrence Berkeley National Laboratory

Berkeley, CA 94720

[2]Department. of Chemistry

Montana State University

Bozeman, MT 59717

May 12, 2009

Abstract

A numerical experiment was carried out to test whether the patchy CO_2 emission patterns observed at the ZERT release facility are caused by the presence of packers that divide the horizontal injection well into six CO_2-injection zones. A three-dimensional model of the horizontal well and cobble-soil system was developed and simulations using TOUGH2/EOS7CA were carried out. Simulation results show patchy emissions for the seven-packer (six-injection-zone) configuration of the field test. Numerical experiments were then conducted for the cases of 24 packers (23 injection zones) and an effectively infinite number of packers. The time to surface breakthrough and the number of patches increased as the number of packers increased suggesting that packers and associated along-pipe flow are the origin of the patchy emissions. In addition, it was observed that early breakthrough occurs at locations where the horizontal well pipe is shallow and installed mostly in soil rather than the deeper cobble. In the cases where the pipe is installed at shallow depths and directly in the soil, higher pipe gas saturations occur than where the pipe is installed slightly deeper in the cobble. It is believed this is an effect mostly relevant to the model rather than the field system and arises through the influence of capillarity, permeability, and pipe elevation of the soil compared to the cobble adjacent to the pipe.

Introduction

The main challenge addressed by the geologic carbon sequestration near-surface monitoring community is how to detect small CO_2 seepage fluxes and anomalous concentrations in the presence of relatively large natural background fluxes caused by biological processes (e.g., Oldenburg et al., 2004; Lewicki et al., 2005; 2007; Leuning et al., 2008; Cortis et al., 2008). The Zero Emissions Research and Technology (ZERT) project established a CO_2 shallow-release facility on the Montana State University campus to carry out experiments aimed at developing capabilities and testing approaches for detecting and monitoring potential CO_2 seepage (Spangler et al., this issue). The 100 m-long horizontal well installed at the site was designed to model a line source of leakage from a geologic carbon sequestration site such as could occur along a leaky fault.

One of the first observations from the experiment arising from careful measurements of CO_2 flux using the accumulation chamber method was that emissions were patchy (i.e., expressed as localized high-flux regions) above the horizontal well (Lewicki et al., 2007; Lewicki et al., this issue; Spangler et al., this issue). This patchy nature of CO_2 emissions flux persisted over two field seasons with little change in patch location. In this study, the origin of the patchy emission pattern observed in the experiment above the nominally horizontal well was investigated. Specifically, numerical experimentation was used to test the hypothesis that high-flux regions at the ground surface are caused by relatively long slightly sloping runs of perforated pipe in which CO_2 flows slightly upward until encountering a packer, at which point it enters the cobble-soil system and migrates vertically upwards with little lateral spreading, to produce a persistent localized area of high CO_2 flux, i.e., a patchy emission pattern.

Background

Observation

Background and overview of the ZERT release facility and related research activities are described fully in Spangler et al. (this issue). The focus of this paper is on numerical experiments that investigate the origin of persistent localized emission regions referred to as patchy emissions. The intriguing motivation for this study is illustrated in Figure 1. Figure 1b shows the elevation of the nominally horizontal well with large vertical exaggeration to amplify the 0.50 m maximum vertical deviation over the 70 m of horizontal injection zones. Also shown are the approximate locations of the seven packers that separate the perforated pipe into the six zones into which CO_2 was injected through tubing. In addition, the figure shows vertical dashed lines that highlight the spatial relationship between packer locations in Figure 1b and soil CO_2 flux maxima measured using the accumulation chamber method along the surface trace of the well (Figure 1a) (Lewicki et al., 2007). A strong correlation is observed between packer locations and the patchy CO_2 emission pattern at the ground surface. This observation led the ZERT team to speculate that the packers block flow within each packed-off zone of the pipe and create effectively a local point-source of CO_2 injection into the formation which then creates a persistent emission-flux and concentration hot spot at the ground surface.

Hypothesis

Formalizing the observations of patchy emissions and their presumed cause discussed above, one can propose the following testable hypothesis: the CO_2 that is injected into each zone of the well flows within the pipe upward by buoyancy forces along the slightly sloping water-filled sections of each zone until it encounters a packer, at which point it accumulates and flows through the

perforations of the pipe into the cobble-soil system effectively forming a local point source of gaseous CO_2. Because the pipe is below the water table, the gas migrates vertically upwards initially through the porous sediments strongly by buoyancy force and retains its focused flow pattern all the way through the vadose zone to the ground surface.

To test this hypothesis, numerical experiments were carried out using a three-dimensional (3D) model of the ZERT release facility. The Base Case model considers the system as it is installed with six packed-off zones. An alternative scenario was simulated with 23 packed-off zones (Case 1), and with effectively continuous injection from the pipe into the formation (Case 2). Both of these alternative scenarios reduce the amount of along-pipe flow that can occur and effectively reduce or eliminate the point-source geometry of the release.

Methods

Numerical Simulation

To carry out the numerical experiment outlined above, the multiphase and multicomponent subsurface transport simulator TOUGH2 (Pruess et al., 1999) was used with EOS7CA, a research module that models the chemical components of interest here, namely water, CO_2, and air (e.g., Oldenburg and Unger, 2003; Oldenburg et al., 2009). TOUGH2 solves implicitly the time-dependent coupled flow and transport equations arising from the integral finite difference method. Non-linearity is handled using Newton's method, and the large set of linear equations arising at each Newtonian iteration is solved using a sparse conjugate gradient solver. Convergence is ensured by the use of a residual-based convergence criterion at each time step. Table 1 presents the equations solved in TOUGH2; full details of the methods used in TOUGH2 can be found in Pruess et al. (1999) available online at the TOUGH2 website. Note the energy equation is omitted from Table 1

because isothermal conditions are assumed in this study. TOUGH2/EOS7CA is designed for near-surface applications and uses Henry's Law for modeling CO_2 solubility. Other TOUGH2 modules (e.g., ECO2N (Pruess, 2005) and EOS7C (Oldenburg et al., 2004) are available for deep subsurface (high-pressure) systems.

Model System and Discretization

Prior simulation studies of the ZERT shallow-release facility (Oldenburg et al., 2009; Spangler et al., this issue) used a two-dimensional (2D) cross-section model (perpendicular to the pipe) known as the transverse model. These prior transverse model simulations were appropriate because of the long sub-horizontal dimension of the pipe and they were useful for estimating breakthrough times, surface fluxes, and the degree of lateral spreading. For this study, aimed at testing the hypothesis that variations in the pipe elevation are the origin of patchy surface emissions, a longitudinal (along-the-pipe) geometry is needed. Furthermore, because the fundamental observation at the ground surface is of patchy emissions, discretization in the transverse direction is also required resulting in the need for a 3D grid.

A conceptual model of the longitudinal *XY* plane (vertical cross section) containing the pipe is shown in Figure 2. As shown, the system consists of a gently sloping ground surface (gradient ~1.7% downward to the northeast) with a 1.2 m-thick soil layer underlain by a cobbly sand (Mokwa, 2006) referred to here as cobble. The water table fluctuates seasonally and is approximated here to be at the level shown in Figure 2 consistent with its location during the summers when experiments have been carried out. Properties of the soil and cobble layers are given in Table 2.

The full 3D grid was generated using the WinGridder package (Pan, 2008). The grid was designed to capture the details of the release of CO_2 from the horizontal well. Assuming for convenience that the release is symmetric about the centerline of the pipe, a grid was constructed for the region to the northwest of the pipe. It is assumed further for simplicity that the topography and soil and cobble layer properties are invariant in the horizontal direction perpendicular to the pipe. The discretization developed represents the horizontal well and its elevation variations in detail as shown by the *XY* (vertical plane) cross section containing the pipe shown in Figure 3. Note in Figure 3 that the pipe is fully within the cobble material in the southwest (SW, left-hand side) and at the cobble-soil interface or within the soil on its northeast (NE, right-hand side) end. The 3D grid consists of 11 replications of the grid shown in Figure 3. Though the pipe discretization is replicated in the direction perpendicular to the pipe (*Z*-direction), there is no pipe material in the model anywhere except in the plane at $Z = 8.975$ m (the mirror plane) and cobble or soil is specified as appropriate even where the discretization mimics the pipe geometry. The resulting 3D grid is shown in Figure 4 with independent scaling of the three axes (the *Z*-direction connections are not shown). Note the fine spacing of the *XY* planes near the well intended to capture the details of processes near the well while the plane spacing increases away from the well where the influence of the injection is much smaller. Observations of the flux pattern from the 2007 release experiment guided our choice of the variable spacing of the multiple vertical planes and the extent of the system perpendicular to the pipe. Each *XY* plane contains 4779 grid blocks; there are 11 planes for a total of 52,569 gridblocks and 147,486 connections.

Boundary conditions are no-flow at the bottom and atmospheric conditions at the top represented by elevation-dependent pressure that is constant with time. The CO_2 concentration boundary condition

at the top is mass fraction in the aqueous phase equal to 5.76×10^{-4} which corresponds to a gas-phase concentration of 380 ppmv and is also the initial condition throughout the system. The sides (X = 0.0 and X = 96.5 m) are closed (no-flow boundary condition), while conditions at the rear XY plane (Z = 4.5 m) are constant with time and equal to the initial condition. The front XY plane (Z = 8.975 m) is a no-flow boundary and serves as the mirror plane of the symmetric model system. All simulations are isothermal at 15 ^{o}C.

Flow Properties of the Materials

The properties used for the two layers (soil and cobble) are given in Table 2. Capillary pressure and relative permeability characteristic curves were approximated to give a higher capillary pressure in the presumably finer-grained soil than in the cobble for a given liquid saturation. The porosity of both layers was set to 0.35, while the permeabilities of the layers were assigned based on a calibration from an earlier release (see Oldenburg et al., 2009; Spangler et al., this issue). Rainfall infiltration was set to zero as the CO_2 releases from the horizontal well were carried out in summer months for which there is little precipitation. The steady-state gravity-capillary equilibrium moisture profile used as the initial condition is shown in Figure 5. Note the dry region around X = 15 m, Y = 8.7 m which arises from a capillary barrier effect (local region of high liquid saturation above lower liquid saturation) that develops in unsaturated systems where finer-grained materials overlie coarser materials (e.g., Oldenburg and Pruess, 1993).

The pipe was approximated as a high-porosity and high-permeability porous medium with low capillarity. This assumption clearly does not allow a rigorous modeling of intra-well flow processes, but will capture the key effect of faster flow and transport of CO_2 within the well and stronger

capillary suction of the formation than the pipe in unsaturated conditions. This is critical as one aspect of the hypothesis being tested is that along-well flow of CO_2 accumulates against packers in the high-elevation regions of each packed-off section. As shown below, the processes of flow in the well are believed to be adequately modeled using the porous-medium approach. The total injection rate of CO_2 into the pipe is 100 kg/d distributed evenly into each packed-off section and divided by two to honor the mirror symmetry of the system. Note that not all zones are the same length and therefore this injection specification differs slightly from that in the field experiment which injected the same amount of CO_2 per unit length. This difference does not affect the conclusions of the numerical experiments presented here.

Results

The basic flow and transport processes involved in the injection of CO_2 beneath the water table into the cobble-soil system at the ZERT release facility have already been described (Oldenburg et al., 2009; Spangler et al., this issue). To summarize briefly, injected CO_2 first displaces water in the saturated zone and forms bubbles which then move upwards by buoyancy into the vadose zone. The buoyancy driving force in the saturated zone is sufficiently large to make CO_2 move upward without significant spreading. In the vadose zone, CO_2 is the dense gas relative to air and therefore tends to spread out, especially in the unsaturated cobble, as it moves upward by pressure gradient forces. Below are presented results of the testing of the hypothesis of the packer origin of patchy emissions for the 3D system, and some observations about moisture redistribution as injected CO_2 creates unsaturated conditions.

Figure 6 presents a 3D view of results for the Base Case at t = 3 days of the mass fraction of CO_2 in the gas phase (X_g^{CO2}). This figure shows the right-hand (northwest) side of a symmetric system with

patchy emissions on the ground surface (approximated as a uniformly sloping surface). The first-order observation is that the Base Case model is able to produce, at least qualitatively, patchy emission patterns similar to those observed in the field. The overall average measured CO_2 flux at t = 9 days is 1.8×10^{-5} kg m^{-2} s^{-1} (1500 g m^{-2} d^{-1}) while the modeled average flux is 2.2×10^{-5} kg m^{-2} s^{-1} (1900 g m^{-2} d^{-1}). The modeled mean fluxes along the projection of the pipe at the ground surface are presented in Table 3 (see also Lewicki et al., 2007). Note that this agreement is considered adequate for purposes here, and system properties are not altered from those used in Oldenburg et al. (2009) to match the measured fluxes. From this point of qualitative match of model and field systems, a numerical experiment may be conducted to test whether packer location and along-pipe flow are the cause of patchy emissions.

The first experimental case (Case 1) considered is one in which there are four times as many packers as actually installed. The idea is to test the possibility that more packers will create more patches. For convenience, results are presented for mass fraction of CO_2 in the gas phase only in the plane containing the pipe, although all of the results presented are from the full 3D model. Shown in Figure 7 are results for the Base Case (six zones) and Case 1 (23 zones) at five times (t = 0.06, 0.5, 1.0, 1.5, and 2.0 days). In the Base Case, there is an early breakthrough at X = 61 m, followed by a breakthrough at X = 84 m. Both of these breakthroughs occur at the upper ends of packer sections suggesting the hypothesis that along-pipe flow of CO_2 and subsequent blocking of flow by the packers produce essentially point-sources. At these locations, the pipe is also very shallow. Other point sources produced by packer locations create additional patches of high CO_2 emissions later in time. It is speculated that the breakthrough at X = 84 m (Zone 1) is not as fast as the one at X = 61 m (from Zone 2) because it has no neighboring zone to the right-hand side and therefore does not

receive any lateral CO_2 flow as occurred at the Zone 2-3 packer. Finally, note that the injection at X > 61 m is into pipe that is within soil, which has larger permeability than cobble as determined by calibration (Oldenburg et al., 2009; Spangler et al., this issue). These factors, namely proximity to surface and pipe installed in high-permeability soil, appear to play a role in the early breakthrough. The patchy emission pattern appears to result from the packer blocking along-pipe flow and causing an effective point-source release.

Results for Case 1 (23 zones) show some of the same behavior as the base case, e.g., tendency for early breakthrough at X = 61 m and 84 m. But the Case 1 results also show clearly the tendency for multiple packers to produce multiple point sources as evidenced by the numerous finger-like CO_2 plumes generated by each packer. From this result, the hypothesis of a packer origin of patchy emissions is confirmed.

The hypothesis is further tested by running a Case 2 with effectively an infinite number of packers in the pipe. Tthis condition is achieved by setting the horizontal permeability of the pipe to 10^{-18} m^2 (effectively zero). Results are shown in Figure 8. Comparing Figures 7 and 8 shows that the more packers used, the less pronounced are any given upward-flowing plumes of CO_2 because each effective point source is weaker. However, the proximity of the pipe to the ground surface still produces early breakthroughs (e.g., at X = 61 m), and the effect of injecting into pipe that is embedded within the soil in the model is to create an area where early breakthrough is independent of packer location or number.

Patchy emissions in the field experiment were persistent throughout the periods of injection. In the model, the patches tend to merge more than in the field experiment. Figure 9 presents results at t = 5 and 9 days showing more merging but also persistence of some patches for the Base Case. This greater persistence of patches in the field suggests that there are features or processes in the field that are not captured in the model. It is speculated that the model system may have a larger horizontal permeability than the actual site, especially if the high permeability of the soil is due to cracks which would tend to be subvertical. The implication of these results for actual GCS seepage monitoring and modeling is that persistent patchy emission patterns may be the expected form of seepage at GCS sites under similar conditions where unexpected low-level CO_2 migration to the near-surface occurs.

Finally, there are some observations of moisture evolution in the 3D system that are worthy of note. The initial moisture distribution in the 3D model changes in two ways as CO_2 is injected. First, CO_2 injected into the pipe increases CO_2 mass fraction in the aqueous phase and eventually exceeds the solubility limit causing two-phase conditions with CO_2 gas displacing water. Second, once unsaturated conditions develop due to CO_2 injection, variations in capillary suction properties of the pipe and adjacent materials affect moisture retention and gas-entry properties. These differences appear along the length of the pipe as shown in Figure 10 by the different liquid saturations present in the pipe in the left-hand side (SW region) and right-hand side (NE region). On the left-hand side of the system (SW region of pipe), the horizontal well pipe is installed at a greater depth and it is in the cobble below the water table prior to CO_2 injection. On the right-hand side of the system (NE end of pipe), the horizontal well is installed shallower and it is in the soil very near the water table. The soil has a stronger capillary suction than the cobble, which all other things being equal, would

result in greater pressure needed by the CO_2 gas to displace water from the soil than from the cobble. In this case, the soil also has higher permeability (see Table 2) and the pipe in the NE region is at higher elevation than the SW region. These effects combine to cause more water to be expelled from the pipe as injection occurs than in the SW regions where the pipe is installed in cobble. The result of these differences is a stronger drying of the pipe material as shown in Figure 10. Note that these effects play no role in the gravity-capillary equilibrium in which the pipe is below the water table because both soil and pipe materials are fully saturated and therefore not subject to different strengths of capillary suction. Because the actual pipe consists of slotted steel rather than porous media as modeled here, the contribution of capillarity to this effect is believed to be largely relevant only to the model and does not play a significant role in controlling the amount of water in the pipe in the field system.

Conclusions

Numerical experiments using TOUGH2/EOS7CA with a 3D grid of the ZERT release facility suggest that along-pipe CO_2 flow in the open injection zones is blocked at packers and enters the cobble or soil effectively as a point source. From these effective point sources, early breakthroughs and persistent patchy emission patterns emerge as observed in two summers of field experiments. Early breakthrough occurs where the pipe is shallow and is enhanced when the pipe is in contact with the high-vertical-permeability soil. An implication of this work for actual GCS leakage monitoring and modeling is that patchy emissions may be the expected style of emission from potential low-flux leakage that might occur from GCS sites under conditions of similar soil and moisture as at the ZERT site. The effects of different capillary suction properties, elevation, and

permeability of materials are manifest as differences in liquid saturation in the pipe when injected CO_2 creates unsaturated conditions in the model system.

Acknowledgment

We thank the entire ZERT team for an exciting and supportive research environment. James Amonette (PNNL) pointed out to the first author the correlation of emission patches with packer locations with a figure similar to Figure 1. Stefan Finsterle and Christine Doughty (LBNL) provided helpful internal review comments. This work was carried out in the ZERT project funded by the Assistant Secretary for Fossil Energy, Office of Sequestration, Hydrogen, and Clean Coal Fuels, through the National Energy Technology Laboratory, U.S. Department of Energy under Contract No. DE-AC02-05CH11231.

References

Corey, Corey, A.T., The interrelation between gas and oil relative permeabilities, *Producers Monthly*, 38-41, November 1954.

Cortis, A., C.M. Oldenburg, and S.M. Benson, The role of optimality in characterizing CO_2 seepage from geologic carbon sequestration sites, *Int. J. Greenhouse Gas Control*, *2*, 640-652, 2008.

Leuning, R., D. Etheridge, A. Luharb, and B. Dunse, Atmospheric monitoring and verification technologies for CO_2 geosequestration, *Int. J. Greenhouse Gas Control 2*(3), 401-414, 2008.

Lewicki, J.L., G.E. Hilley, L. Dobeck, and L. Spangler, Dynamics of CO2 concentrations and fluxes during a shallow subsurface CO2 release experiment, *Env. Earth Sci*., this issue.

Lewicki, J.L., C.M. Oldenburg, L. Dobeck, and L. Spangler, Surface CO_2 leakage during the first shallow subsurface CO_2 release experiment, *Geophys. Res. Lett., 34, L24402, 2007.*

Mokwa, R., Subsurface exploration for the MSU CO_2 injection project—Phase I, unpublished report, Montana State University, Civil Engineering Department, 2006.

Oldenburg, C.M., J.L. Lewicki, L. Dobeck, and L. Spangler, Modeling gas transport in the shallow subsurface during the ZERT CO_2 release test, Transport in Porous Media, in press, available online DOI 10.1007/s11242-009-9361-x.

Oldenburg, C.M., and K. Pruess, On numerical modeling of capillary barriers, *Water Resour. Res.*, *29*(4), 1045–1056, 1993.

Oldenburg, C.M., G.J. Moridis, N. Spycher, and K. Pruess, EOS7C Version 1.0: TOUGH2 Module for Carbon Dioxide or Nitrogen in Natural Gas (Methane) Reservoirs, Lawrence Berkeley National Laboratory Report LBNL-56589, March 2004 (http://www-esd.lbl.gov/TOUGHPLUS/manuals/TOUGH2-EOS7C_Users_Guide.pdf)

Oldenburg, C.M., J.L. Lewicki, and R.P. Hepple, Near-surface monitoring strategies for geologic carbon dioxide storage verification, Lawrence Berkeley National Laboratory Report *LBNL-54089*, October 2003.

Oldenburg, C.M., and J.L. Lewicki, On leakage and seepage of CO_2 from geologic storage sites into surface water, *Env. Geol., 50*(5), 691-705, 2006.

Oldenburg C.M., and A.J.A. Unger, On leakage and seepage from geologic carbon sequestration sites: unsaturated zone attenuation. *Vadose Zone Journal 2*, 287-296, 2003.

Pan, L., User information for WinGridder Version 3.0, (May 30, 2008). Lawrence Berkeley National Laboratory. Paper LBNL-273E. http://repositories.cdlib.org/lbnl/LBNL-273E

Pruess, K., C. Oldenburg, and G. Moridis, *TOUGH2 User's Guide, Version 2.0*, Lawrence Berkeley National Laboratory Report *LBNL-43134*, November 1999.

Pruess, K, ECO_2N: A TOUGH2 fluid property module for mixtures of water, NaCl, and CO_2, Lawrence Berkeley National Laboratory Report *LBNL-57952*, August 2005, (http://esd.lbl.gov/TOUGH2/ecO_2n_man.pdf)

Spangler, L. et al., A shallow subsurface controlled release facility in Bozeman, Montana, USA, for testing near surface CO_2 detection techniques and transport, Env. Earth Sci., this issue.

van Genuchten, M.Th, A closed-form equation for predicting the hydraulic conductivity of unsaturated soils, *Soil Sci. Soc., 44*, 892-898, 1980.

Nomenclature

d	molecular diffusivity	$m^2\ s^{-1}$
g	acceleration of gravity vector	$m\ s^{-2}$
F	Darcy flux vector	$kg\ m^2\ s^{-1}$
k	permeability	m^2
k_r	relative permeability	
M	mass accumulation term	$kg\ m^{-3}$
n	outward unit normal vector	
NK	number of components	
NPH	number of phases	
P	total pressure	Pa
P_c	capillary pressure	Pa
q	mass flux	$kg\ m^{-2}\ s^{-1}$
q_v	volumetric source term	$kg\ m^{-3}\ s^{-1}$
S	saturation.	
t	time	s
T	temperature	^oC
V	volume	m^3
X	mass fraction with phase subscript and component superscript	
X	X-coordinate	
Y	Y-coordinate	
Z	Z-coordinate (positive upward)	

Greek symbols

α	$1/P_0$ in van Genuchten's capillary pressure function	Pa^{-1}
β	phase index (subscript)	
Γ	surface area	m^2

θ	exponent for temperature dependence of diffusivity		
κ	mass components (superscript)		
λ	van Genuchten's m	-	
μ	dynamic viscosity	kg m^{-1} s^{-1}	
ρ	density	kg m^{-3}	
τ	tortuosity		
ϕ	porosity		

Subscripts and superscripts

g	gas
l	liquid
s	satiated (saturation)
max	maximum
r	residual
w	water
0	reference value

Tables

Table 1. Governing equations solved in TOUGH2/EOS7CA for isothermal problems.

Description	Equation
Conservation of mass	$\frac{d}{dt}\int_{V_n} M^\kappa dV = \int_{\Gamma_n} \mathbf{F}^\kappa \cdot \mathbf{n} d\Gamma + \int_{V_n} q_v{}^\kappa dV$
Mass accumulation	$M^\kappa = \phi \sum_{\beta=1}^{NPH} S_\beta \rho_\beta X_\beta{}^\kappa$
Phase flux	$\mathbf{F}_\beta = -k \frac{k_{r\beta}\rho_\beta}{\mu_\beta}\left(\nabla P_\beta - \rho_\beta \mathbf{g}\right)$
Component flux	$\mathbf{F}^\kappa = \sum_{\beta=1}^{NPH} \left(X_\beta{}^\kappa \mathbf{F}_\beta - \phi \tau_o \tau_\beta \rho_\beta d_\beta^k \nabla X_\beta{}^\kappa \right)$
Pressure and capillary pressure	$P_\beta = P + P_{c\beta}$
Henry's law	$P_g^\kappa = K_H x_{aq}^\kappa$
Relative permeability (liquid after van Genuchten, 1980; gas after Corey, 1954)	$if\ S_l < S_{ls},\quad k_{rl} = \sqrt{S^*}\left\{1-\left(1-\left[S^*\right]^{1/\lambda}\right)^\lambda\right\}^2$ $if\ S_l \geq S_{ls} \quad k_{rl} = 1$ $if\ S_{gr} = 0 \quad k_{rg} = 1 - k_{rl}$ $if\ S_{gr} > 0 \quad k_{rg} = \left(1-\hat{S}\right)^2\left(1-\hat{S}^2\right)$ $where\ S^* = \left(S_l - S_{lr}\right)/\left(S_{ls} - S_{lr}\right),$ $\hat{S} = \left(S_l - S_{lr}\right)/\left(1 - S_{lr} - S_{gr}\right)$
Capillary pressure (after van Genuchten, 1980)	$P_c = P_0\left(\left[S^*\right]^{-1/\lambda} - 1\right)^{1-\lambda}$ $subject\ to - P_{\max} \leq P_c \leq 0$
Molecular diffusion	$f_\beta^\kappa = -\phi \tau_o \tau_\beta \rho_\beta d_\beta^k \nabla X_\beta{}^\kappa$ $where\ \tau_o \tau_\beta = \tau_o k_{r\beta}(S_\beta)$ and $d_\beta^k(P,T) = d_\beta^k(P_0,T_0)\frac{P_0}{P}\left[\frac{T+273.15}{273.15}\right]^\theta$

Table 2. Properties of the materials in the model.

	Soil	Cobble	Pipe
Temperature (T)	15 ^{o}C	15 ^{o}C	15 ^{o}C
Porosity (ϕ)	0.35	0.35	0.99
Permeability (k)	5×10^{-11} m^2	3.2×10^{-12} m^2	1×10^{-10} m^2
Capillary Pressure (P_c)	van Genuchten[1,2] $\lambda = 0.291$, $S_{lr} = 0.15$, $\alpha = 2.04 \times 10^{-4}$ Pa^{-1}, $P_{max} = 5 \times 10^5$ Pa, $S_{ls} = 1$.	van Genuchten[1,2] $\lambda = 0.627$, $S_{lr} = 0.10$, $\alpha = 1.48 \times 10^{-3}$ Pa^{-1}, $P_{max} = 5 \times 10^5$ Pa, $S_{ls} = 1$.	No capillary pressure
Relative permeability (k_r)	Liquid: van Genuchten[1,2]; Gas: Corey[3] $S_{lr} = 0.17$, $S_{gr} = 0.05$	Liquid: van Genuchten[1,2]; Gas: Corey[3] $S_{lr} = 0.12$, $S_{gr} = 0.05$	Linear with saturation[1] $S_{lr} = 0.1$, $S_{gr} = 0.05$
Molec. diffusivity coefficients (d_β^κ)	Liquid: 10^{-10} m^2 s^{-1} Gas: 10^{-5} m^2 s^{-1} $\theta = 1.0$, $P_0 = 10^5$ Pa	Liquid: 10^{-10} m^2 s^{-1} Gas: 10^{-5} m^2 s^{-1} $\theta = 1.0$, $P_0 = 10^5$ Pa	Liquid: 10^{-10} m^2 s^{-1} Gas: 10^{-5} m^2 s^{-1} $\theta = 1.0$, $P_0 = 10^5$ Pa
Tortuosity (τ_0)	1.0	1.0	1.0
Saturation-dependent tortuosity (τ_β)	Equal to relative permeability	Equal to relative permeability	Equal to relative permeability

[1]Pruess et al. (1999)

[2]λ is m in van Genuchten, 1980.

[3]Corey (1954)

Table 3. Measured and modeled ground-surface fluxes above the pipe at t = 9 days.

Zone	Measured surface flux kg m^{-2} s^{-1}		Modeled surface flux kg m^{-2} s^{-1}	
	Mean	Maximum	Mean	Maximum
1	9.88E-07	3.22E-06	5.52E-06	1.17E-05
2	2.32E-06	7.05E-06	4.64E-06	2.65E-05
3	2.56E-06	1.71E-05	2.87E-06	6.63E-06
4	2.36E-06	5.75E-06	1.14E-06	1.85E-06
5	1.18E-06	1.21E-05	8.56E-07	2.01E-06
6	1.45E-06	6.53E-06	1.91E-06	2.53E-06

Figures

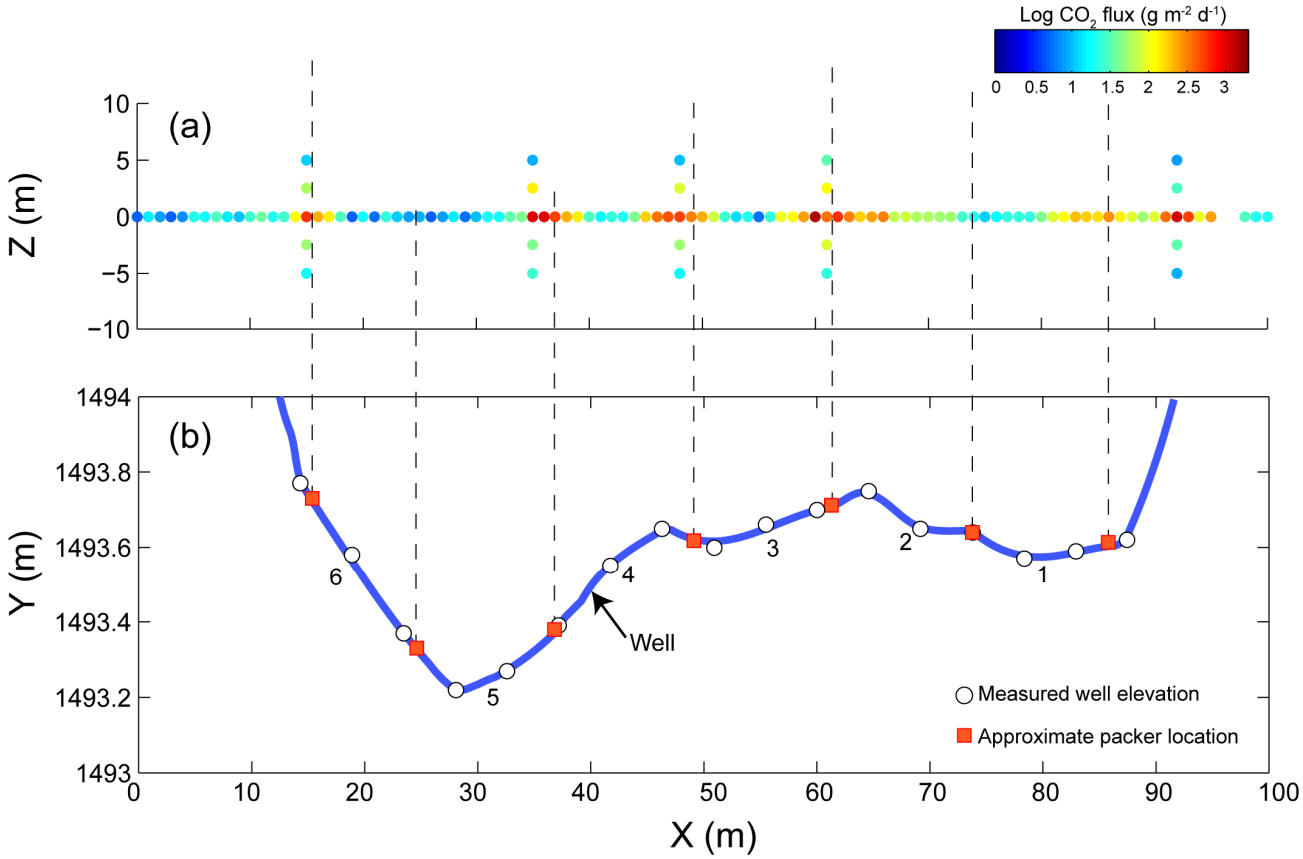

Figure 1. (a) Log soil CO_2 fluxes measured along surface trace of well on day 9 of the first CO_2 release carried out in 2007 (see Lewicki et al., 2007). (b) Elevation of nominally horizontal well (note vertical exaggeration) and packer locations (figure after Amonette, pers. commun.). Focused areas of high CO_2 flux (patches) are generally correlated with packer locations.

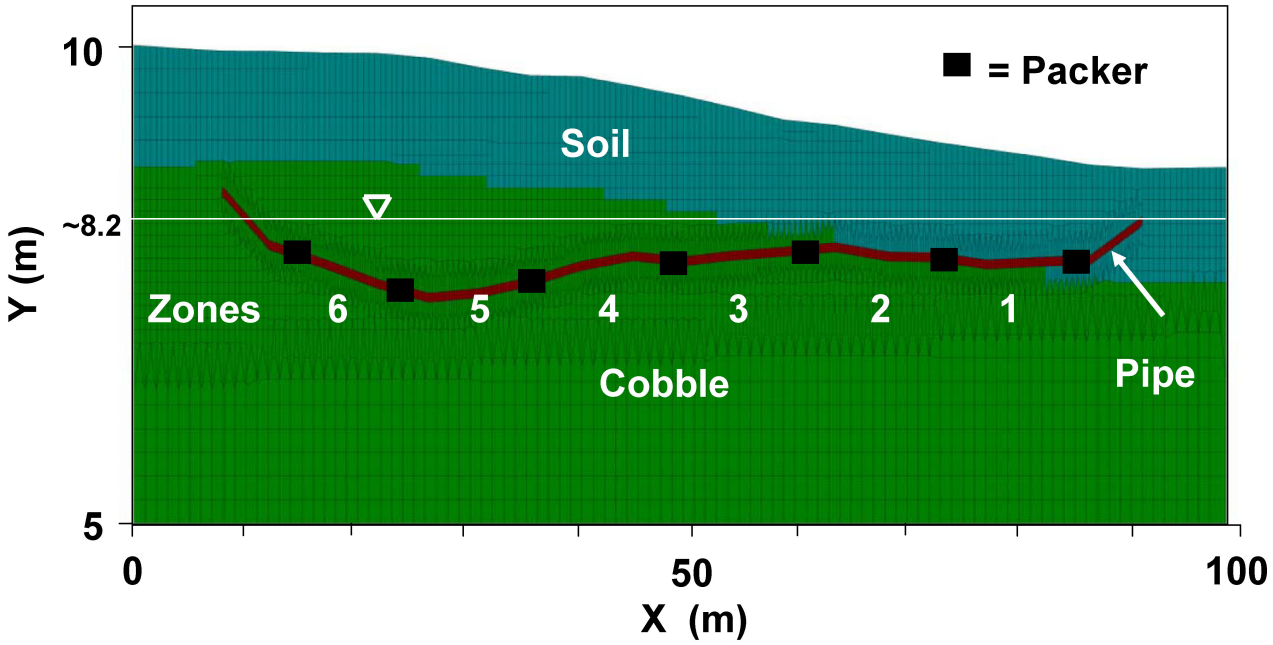

Figure 2. Two-dimensional slice of the three-dimensional model showing soil and cobble layers, water table, packer locations, and injection zone numbering.

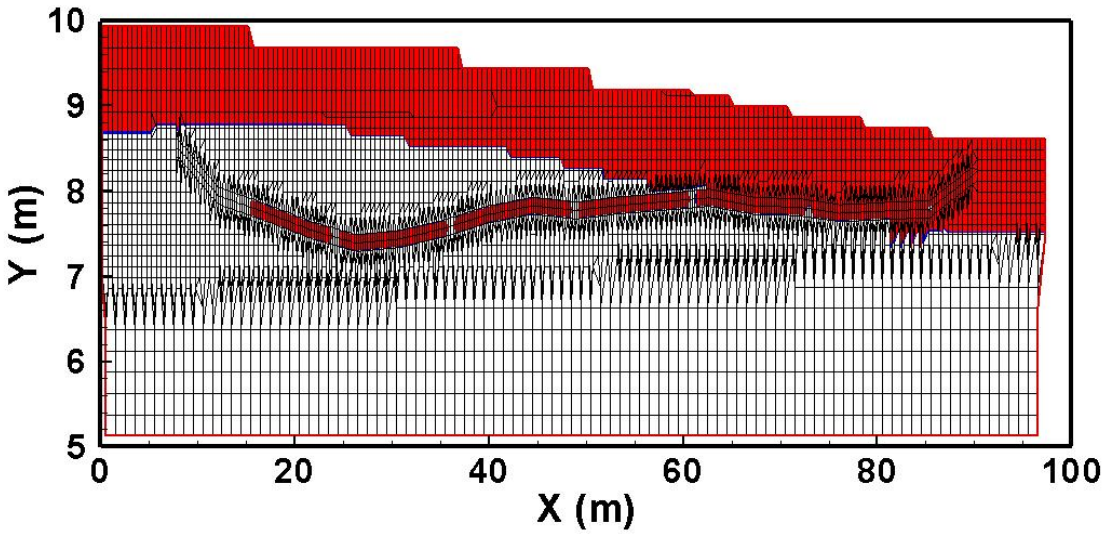

Figure 3. Two-dimensional slice of the three-dimensional model showing the connections between gridblocks. High-permeability regions are shaded (red) showing the open sections of the pipe and the soil layer.

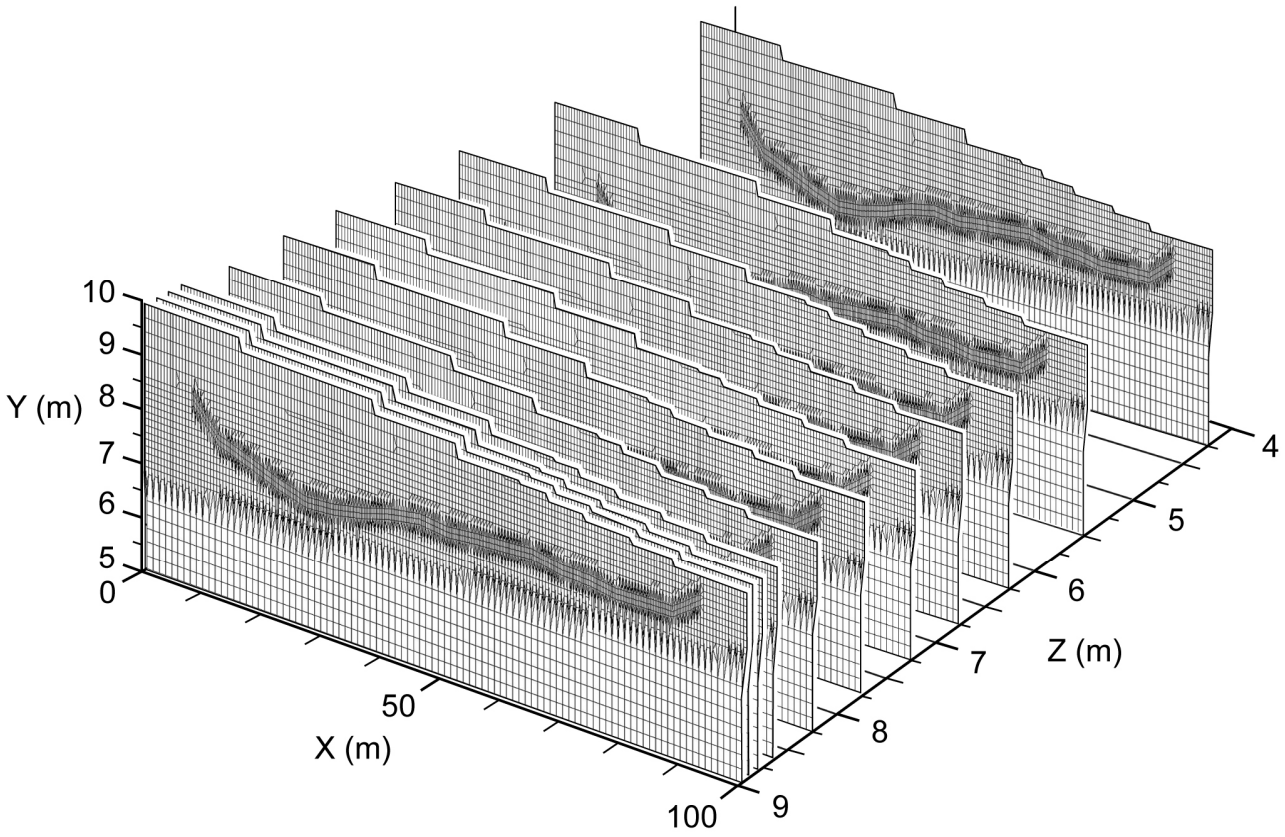

Figure 4. Three-dimensional grid showing the plane at Z = 8.975 m (mirror plane) that contains the pipe and the ten planes to the right-hand side (northwest). Horizontal Z-direction connections between planes are not shown. Note that the pipe discretization is in all planes. However, the only pipe material is in the plane at Z = 8.975 m, while all other planes consist of either soil or cobble depending on location.

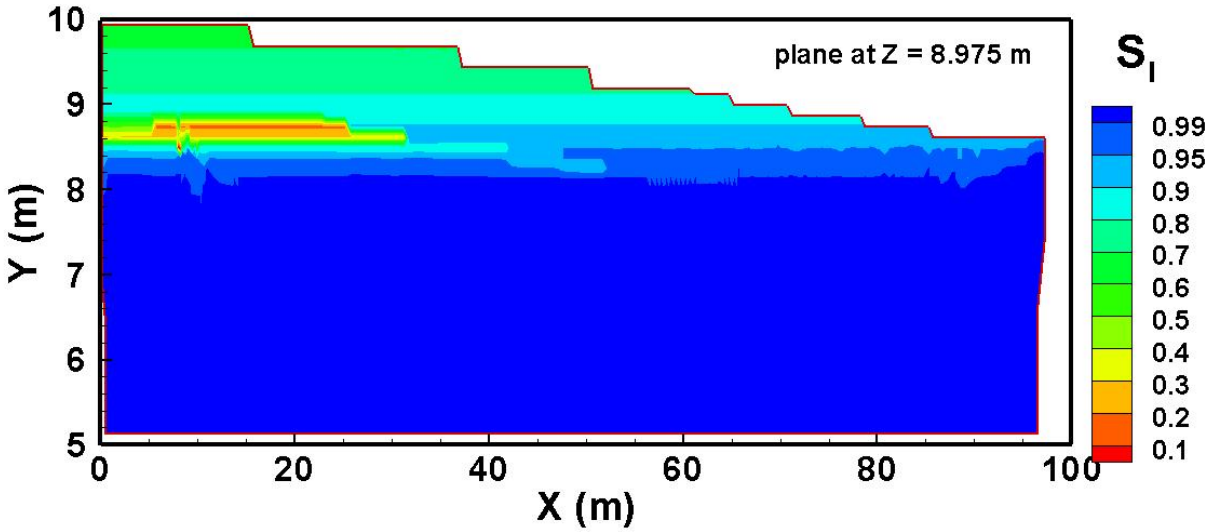

Figure 5. Initial condition of water saturation. Conditions are assumed uniform in the third dimension (*Z*-direction, into the page).

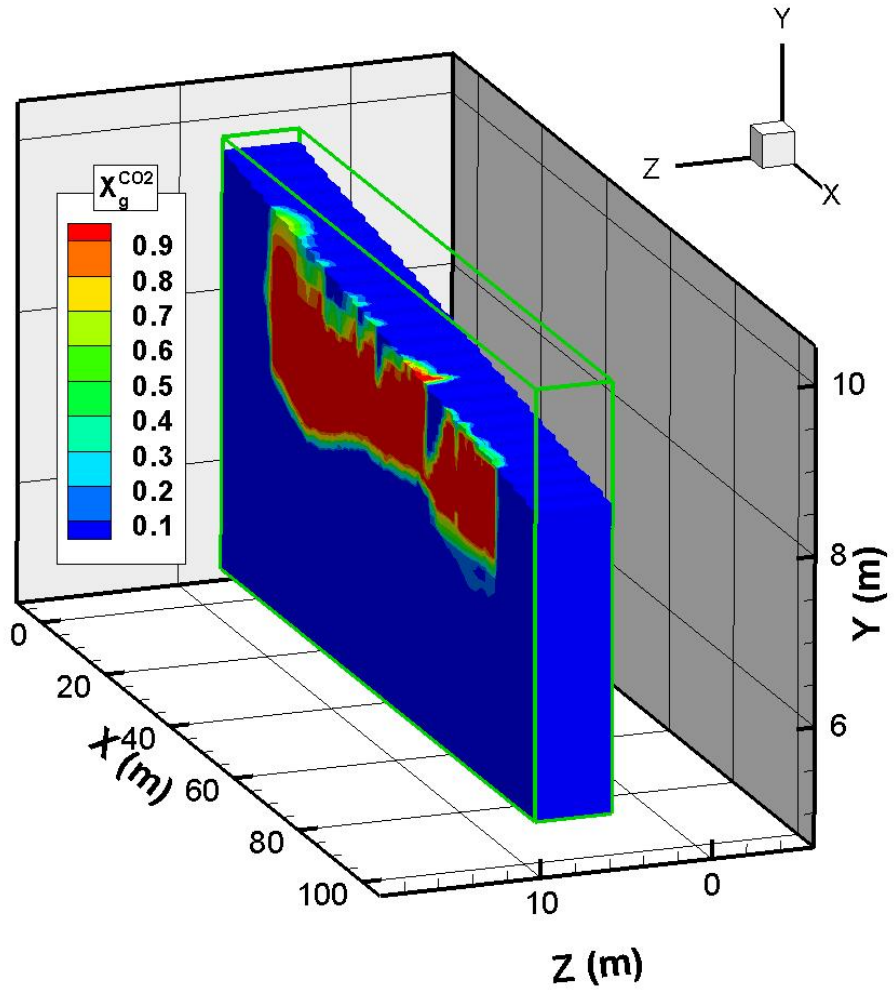

Figure 6. Three-dimensional result of the Base Case showing mass fraction of CO_2 in the gas phase (X_g^{CO2}) in a patchy emission pattern at t = 3 days.

1

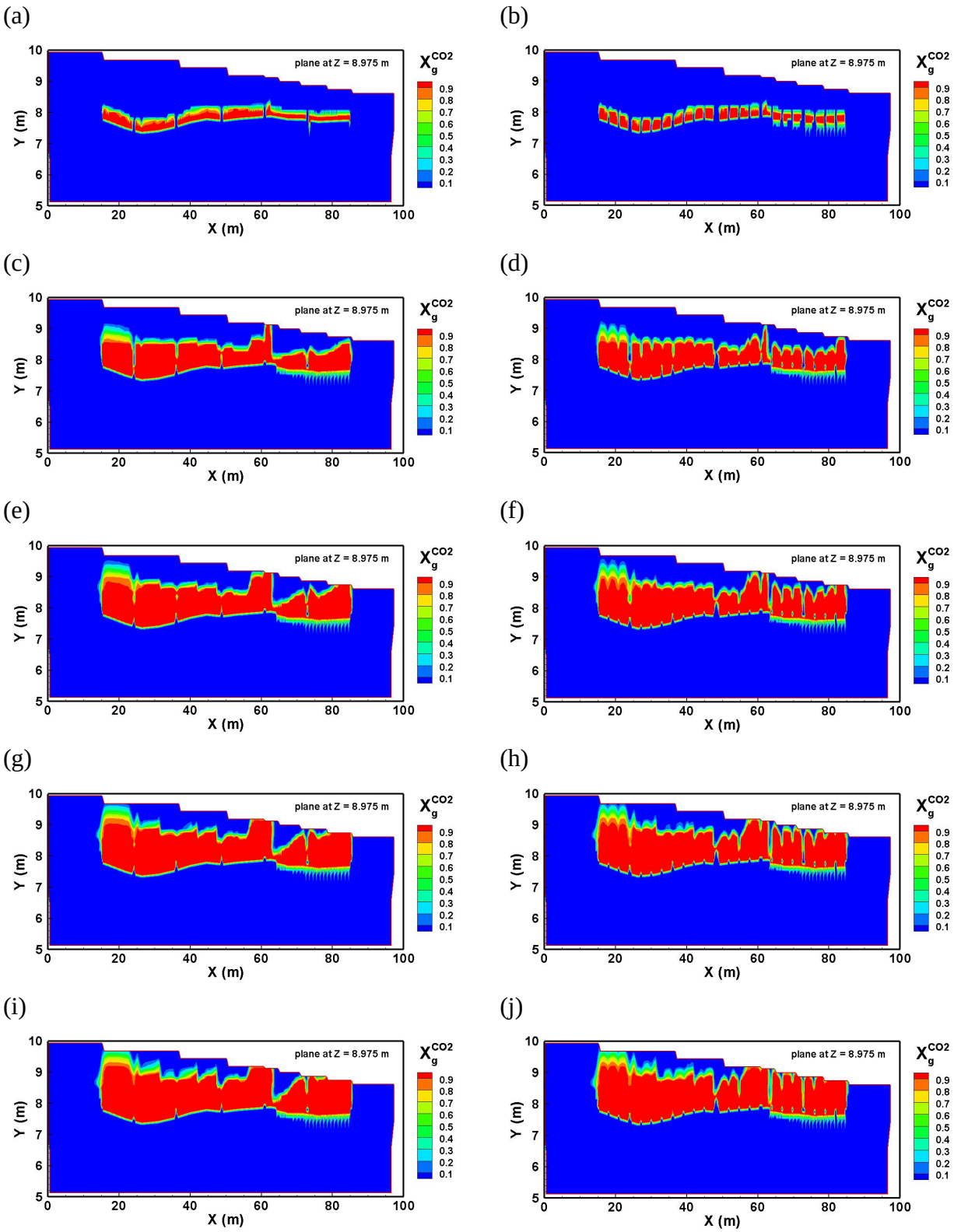
(a)
(b)
(c)
(d)
(e)
(f)
(g)
(h)
(i)
(j)
plane at Z = 8.975 m
X_g^{CO2}
0.9
0.8
0.7
0.6
0.5
0.4
0.3
0.2
0.1
Y (m)
X (m)
5
6
7
8
9
10
0
20
40
60
80
100

Figure 7. Mass fraction of CO_2 in the gas phase at t = 0.06, 0.5, 1, 1.5, and 2 days for the case of injection into six zones (right-hand side(a, c, e, g, i) and 23 zones (left-hand side (b, d, f, h, j)).

(a) (b)

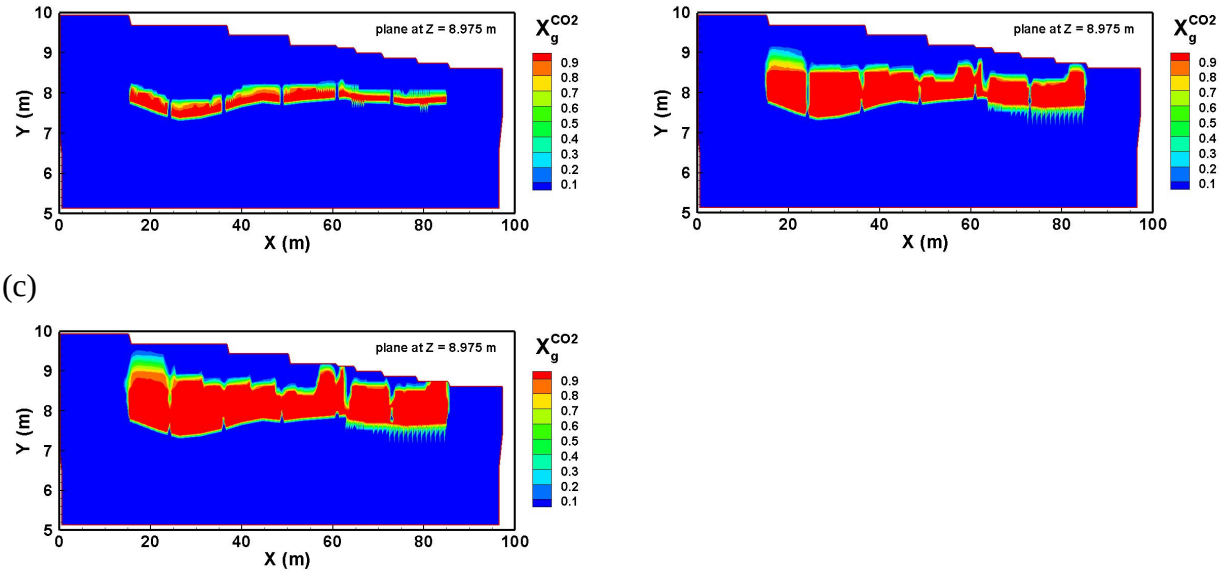

(c)

Figure 8. Mass fraction of CO_2 in the gas phase at t = 0.06, 0.5, and 1 days for the case of injection into an infinite number of zones (spatially continuous injection).

(a) (b)

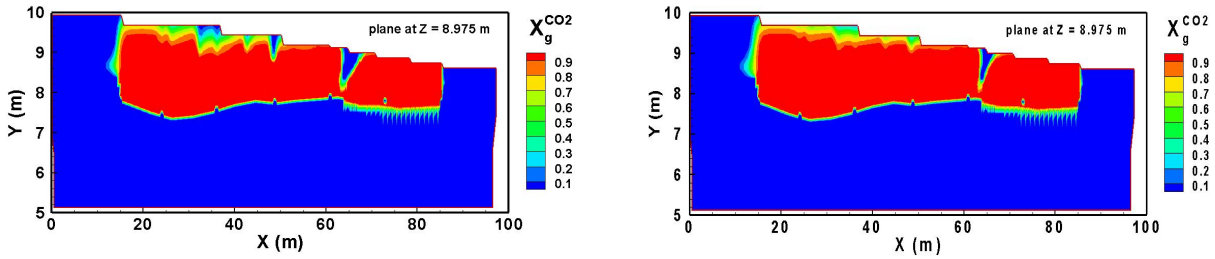

Figure 9. Mass fraction of CO_2 in the gas phase at t = 5, and 9 days for the Base Case showing the merging of some early patches but also patchy emission persistence.

(a) (b)

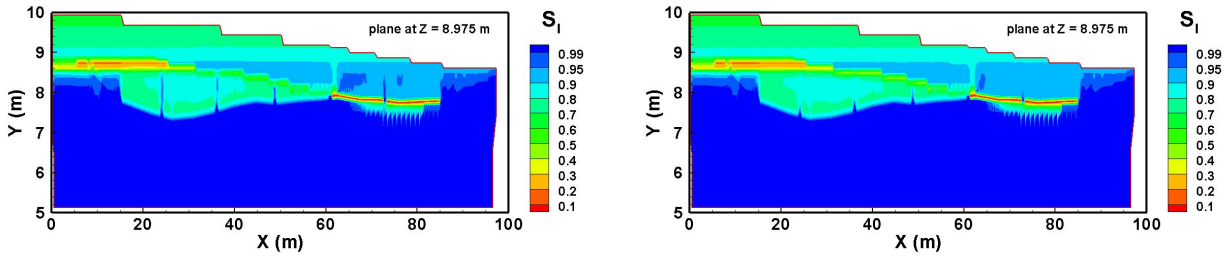

Figure 10. Liquid saturation in the plane Z = 8.975 m at t = 0.5 and 2 days.